ELSEVIER

19 September 1997

Chemical Physics Letters 276 (1997) 255–262

CHEMICAL PHYSICS LETTERS

Mechanisms of atomic and molecular recombination and collision-induced dissociation

Russell T Pack, Robert B. Walker, Brian K. Kendrick

Theoretical Division (T-12, MS B268), Los Alamos National Laboratory, Los Alamos, NM 87545, USA

Received 7 May 1997; in final form 9 July 1997

Abstract

Despite some evidence to the contrary, current chemical kinetics textbooks assume that atomic and molecular recombination and collision-induced dissociation (CID) occur only via sequences of two-body collisions. In this work an approximate quantum method treating all mechanisms simultaneously and on equal footing is used to calculate cross sections for the reaction $Ne_2 + H \rightleftharpoons Ne + Ne + H$. The results provide the first clear quantum evidence that direct three-body as well as sequential two-body collision mechanisms do contribute significantly to recombination and CID. © 1997 Elsevier Science B.V.

1. Introduction

The overall equation for any atomic and molecular recombination reaction is

$$A + B + M \rightarrow AB + M, \tag{1}$$

where A and B are any atoms, molecules, or radicals for which AB has bound states, and M is any species that can carry away the excess energy. In the present work we consider cases in which M is sufficiently inert that contributions of species AM and BM are negligible. Then, all the chemical kinetics textbooks we have seen and most research papers assume that Reaction (1) proceeds only via a sequence of two-body collisions, i.e., by the Lindemann energy transfer (ET) mechanism [1–3],

$$A + B \rightleftharpoons AB^*, \tag{2}$$

$$AB^* + M \rightarrow AB + M. \tag{3}$$

Here the species AB^* represents metastable intermediates.

Do direct three-body collisions also contribute significantly to Reaction (1)? Some [4] have argued that they do not; others [5] have argued that they do, but the evidence until now is sparse, and much of it consists only of hints. The first such hint is collision-induced dissociation (CID),

$$M + AB \rightarrow A + B + M, \tag{4}$$

which is the reverse of Reaction (1). Time-reversal invariance requires that Reactions (1) and (4) involve exactly the same mechanism. Hence, if recombination proceeds only via a sequence of two-body collisions, then CID must proceed only by exactly the reverse sequence of two-body collisions, and that seems physically unlikely to us.

Second, treating the kinetics of Eqs. (1)–(3), one finds that the three-body (3B) mechanism gives pure third-order kinetics. Assuming steady-state (but *not* equilibrium) concentrations of the AB^*, one finds that, at low M pressures, the ET mechanism also

PII S0009-2614(97)00879-8

gives third-order kinetics, but, at high pressures, the ET contribution from any AB^* with a significant lifetime flattens out to become second order. Such behavior is called "falloff" [1]. When AB is a large polyatomic molecule, the recombination kinetics is observed [1] to become second order (and the CID rate unimolecular) for a large range of high pressures implying that the 3B rates are small compared to the ET rates in such cases. However, when A and B are simple atoms, third-order kinetics is observed [1] at all experimental pressures. That implies that atomic recombination is dominated by 3B collisions (and/or AB^* with very short lifetimes). When one of A and B is a diatom and the other an atom or diatom, some falloff is observed but the effective second-order rate constant still rises steeply at the highest experimental pressures [1,2]. That implies that AB^* with significant lifetimes and 3B collisions (and/or AB^* with very short lifetimes) are both making significant contributions, and calculations [3] using only the ET mechanism then give too much falloff.

Third, the orbiting resonance (ET) theory of atomic recombination of Roberts, Bernstein, and Curtiss (RBC) [4] identifies the AB^* as resonant quasibound states trapped behind an angular momentum barrier. RBC [4] did detailed calculations but assumed equilibrium concentrations for all contributing AB^*. If one uses their data but assumes the more accurate steady-state approximation, the resulting rates [6] for the recombination of H atoms in He do show curvature in disagreement with experiment [1]. Furthermore, the calculated [7] ortho-para ratio of the recombined H_2 is in clear disagreement with experiment [8].

The fourth and until now the strongest type of evidence for direct 3B collisions comes from classical mechanics. The quasibound states of the RBC theory are formed by quantum tunneling. However, their classical analogs act like bound states and can only form via direct 3B collisions. Despite this, classical calculations of both recombination [9] and CID [10] agree with experiment! An excellent example is Schwenke's study of the recombination of H atoms in H_2: His calculations [11] using the RBC (ET) theory disagree with experiment; his totally classical calculations [12] agree with experiment. He concludes [12], "the fundamental assumption ..., that recombination takes place predominantly via a sequence of bimolecular collisions, is invalid. ... direct recombination due to three body collisions is the dominant pathway". Unfortunately, his work and conclusion have received little notice.

No quantum calculations clearly distinguishing the ET and 3B mechanisms have been reported, but work is being done in that direction [13–15]. The closest is the work of Pan and Bowman [15] on the CID of HCO by Ar. They see both resonant and direct nonresonant contributions with the resonant dominating, but the resonances included are vibrational resonances; their approximations omit some key rotational motions and resonances.

In this Letter we report the first quantum calculations of recombination and CID in the full three-dimensional space to distinguish the mechanisms.

2. Theory

We consider the case in which A, B, and M are all atoms and use the set of Jacobi coordinates in which $\boldsymbol{r}$ is the vector from A to B, $\boldsymbol{R}$ is the vector from the center of mass of AB to M and γ is the angle between $\boldsymbol{r}$ and $\boldsymbol{R}$. We treat both the vibrational and rotational motion of AB in the infinite order sudden (IOS) approximation. This VRIOS approximation was described by Pfeffer [16] and is an extension of the RIOS approximation [17]. When the bound vibrational levels of AB are widely spaced in energy, the VRIOS approximation is crude except at high energies. However, when the levels are closely spaced, it gives qualitative to semiquantitative accuracy, and it treats all bound and continuum states of AB simultaneously and on the same footing.

Calculations using the VRIOSA, described in more detail elsewhere [6], proceed as follows: r and γ are held fixed while a one-dimensional radial equation in R is solved to generate phase shifts $\eta(r,\gamma)$ for a set of values of r, γ, and partial wave and energy parameters. Then, an r and γ-dependent transition matrix is formed, and its matrix elements between all the desired vibrational wavefunctions are calculated. These matrix elements are well defined if at least one of the vibrational wavefunctions is square integrable. The resulting γ-dependent transition matrix is then used in the RIOS formulas [17], and all the usual simplifications obtain. If the initial and

final states are both bound, the usual integral cross sections σ are obtained, but if one is a continuum state of AB (we use delta function normalization in k, the wavenumber for motion of A relative to B), the usual integral cross section formula yields $d\sigma/dk$ for the transition. Integration over k yields the bound-free integral cross section.

One of the advantages of the VRIOSA here is that it yields an exactly unitary scattering matrix, and the completeness relation gives [6,17] a very simple formula for the total integral cross section that provides a check on the convergence and completeness of the state-to-state results.

3. Calculations and results

The specific system we studied was

$$Ne_2 + H \rightleftharpoons Ne + Ne + H, \quad (5)$$

that is, $A = B =$ Ne and $M =$ H. It is a real system but simple enough to allow calculations. Although Ne_2 lacks the deeply bound states of a chemically bound molecule, the reaction mechanism should be relevant to chemically bound molecules because deeply bound states are accessed only by rovibrational relaxation anyway. H atoms were chosen as the third body because NeH has no bound or quasibound states, so that only the 3B and ET mechanisms are possible. The isotope ^{18}Ne was chosen because it was found that, for the more common isotope, the diatom $^{20}Ne_2$ is extraordinary in that it has a state $(v,j) = (2,0)$ which is bound by only 0.032 Kelvin [18] and whose wavefunction extends to such large distances and couples so well to the 3B continuum as to make it less representative. $^{18}Ne_2$ lacks that state, but its levels are spaced closely enough that the VRIOSA is expected to be fully qualitatively to semiquantitatively accurate. For this system we measure energies in Kelvin (K), i.e., E/k_B, where k_B is Boltzmann's constant.

The potential energy surface for the Ne_2H system was taken to be the pairwise additive sum of interatomic potentials. This approximation should be accurate to a few percent because the non-additive three-body terms largely cancel [19] for these weak van der Waals interactions. We use the best empirical pair potentials available, namely, the Aziz-Slaman [18] Ne_2 potential, which has a well depth of 42.25 K, and the Tang-Toennies [20] NeH potential, which has a well depth of 17.29 K.

Table 1
Properties of the long-lived states of $^{18}Ne_2$

State	(v,j)	E/k_B (K)	τ_{max}(ps)	Γ/k_B (K)	Type
1	(0,0)	−23.56	∞	0	bound
2	(0,2)	−22.08	∞	0	bound
3	(0,4)	−18.65	∞	0	bound
4	(0,6)	−13.33	∞	0	bound
5	(0,8)	−6.23	∞	0	bound
6	(1,0)	−3.63	∞	0	bound
7	(1,2)	−2.72	∞	0	bound
8	(1,4)	−0.69	∞	0	bound
9	(k,2)	0.12	36.24	0.20	barrier slowing
10	(k,4)	0.48	5.02	0.65	barrier slowing
11	(1,6)	1.98	78.18	0.39	QB
12	(k,8)	5.33	9.64	3.17	BAB
13	(0,10)	2.44	5.2e6	5.9e − 6	QB
14	(k,10)	9.48	3.01	10.17	BAB
15	(0,12)	12.15	95.62	0.32	QB
16	(k,14)	22.76	10.55	2.90	BAB
17	(k,16)	34.98	3.77	8.10	BAB
18	(k,18)	48.95	1.92	15.90	BAB

In a first step, all the states of $^{18}Ne_2$ were accurately calculated numerically. The energies and wavefunctions were obtained with the renormalized Numerov method [21], and the lifetimes (time delays) were directly calculated with the log derivative method [21,22]. The properties of all 18 long-lived states are shown in Table 1. There are 8 bound states, 3 quasibound (QB) states, 5 broad above barrier (BAB) resonances, and two resonances caused by slowing by a broad low barrier. Only even j occurs because ^{18}Ne is a spinless boson. The efolding lifetime τ_e of the resonances is one-fourth the maximum lifetime τ_{max} in the table, and the width is $\Gamma = \hbar/\tau_e$ [23].

We note that $^{18}Ne_2$ has 2 QB states with τ_e short enough to contribute significantly to the ET mechanism (the third forms too slowly). Hence, the ET rate for Ne_2 should be of the same order of magnitude as that for H_2, the prototype of the RBC ET theory, because H_2 has only 6 QB states with energies low enough and lifetimes short enough to contribute significantly to its ET rate [4].

The wavefunctions of two Ne_2 states with $j = 10$ are in Fig. 1; they are plotted about their energies and superimposed on a plot of the effective potential. The lower of these is the (0,10) state, a very narrow (long-lived) QB state. The amplitude of the wavefunction in the well region is so much larger than its amplitude outside that its oscillations at large r are too small see on this plot. The higher energy wavefunction is for the $(k,10)$ BAB resonance; it hardly looks resonant at all.

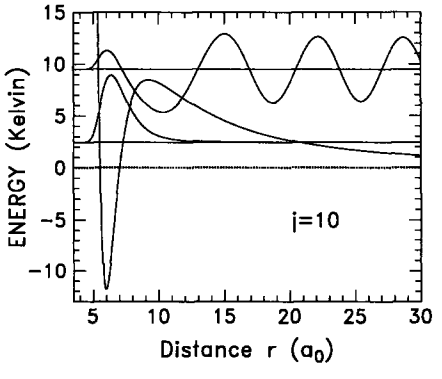

Fig. 1. Effective potential (in Kelvin) versus r (in atomic units) for Ne_2 for $j = 10$. Superimposed on it are plots of two continuum vibrational wavefunctions: A very narrow quasibound state and a broad above barrier resonant state. See text for discussion.

The easier way to find broad resonances is via plots, such as those in Fig. 2, of the collision lifetime versus energy. In Fig. 2(a), one sees very clearly the BAB resonance $(k,10)$. One also sees the sharp spike of the (0,10) QB state; its maximum, listed in Table 1, is 6 orders of magnitude above the top of this plot. Fig. 2(b) shows the $j = 2$ lifetime; it has a peak at very low energies. This resonance is simply caused by slowing due to the broad barrier; the wavefunction at small r is always very small. Note that, in both parts of this figure, τ is negative over large energy ranges. τ is the difference between the total lifetime of the interaction and the time it would take the atoms to pass each other if the interaction were zero, and these negative, nonresonant regions mean that the collisions are taking less time than if there were no interaction. At the energy of the BAB $(k,10)$ resonance, we estimate the zero-interaction passage time to be about 8 ps. Hence, the additional maximum lifetime of 3 ps due to the resonance does not even double this passage time, and that is why its wavefunction in Fig. 1 shows little enhancement.

The second part of the calculation is the VRIOS determination of the $H + Ne_2$ cross sections. The relative collision energy chosen was $E/k_B = 30$ K. This is the most probable collision energy at a temperature of 30 K, where physically one can get a significant concentration of Ne_2 dimers. The phase shifts $\eta(r,\gamma)$ were calculated using the log derivative method [21] and propagating R from 0 to 40 bohr. They were calculated (using symmetry) at 50 of the points of a 100 point Gaussian quadrature in γ, at 81 values of r ranging from 3.5 to to 20 bohr, and partial waves l from 0 to 25. The radial integrals were performed using Simpson's rule quadratures.

Some resulting $d\sigma/dk$ are plotted versus k in Fig. 3 for transitions from all the bound states into the continuum. k is the wavenumber in atomic units for the final relative Ne-Ne motion. The maximum value (2.3) of k in these plots corresponds to a Ne-Ne relative energy of about 50 K. For $j_f = 10$ the spike due to the (0,10) QB resonance is clearly visible in Fig. 3(a) (its peak reaches above this plot to 5×10^7), and the contribution of the BAB resonance is also clearly visible. These peaks correspond directly to those in Fig. 2(a). However, for $j_f = 2$

Fig. 3(b) does not correspond with Fig. 2(b): Because its wavefunction does not penetrate to small r, the low energy $j = 2$ resonance does not contribute to the bound-free scattering; all the contributions here are due to nonresonant, direct 3B collisions. For the other j_f values (not shown), the contributions for 0 and 4 are (like 2) due to direct 3B scattering; for $j_f = 6$ and 12 the QB resonances overlay contributions from BAB resonances and the 3B continuum;

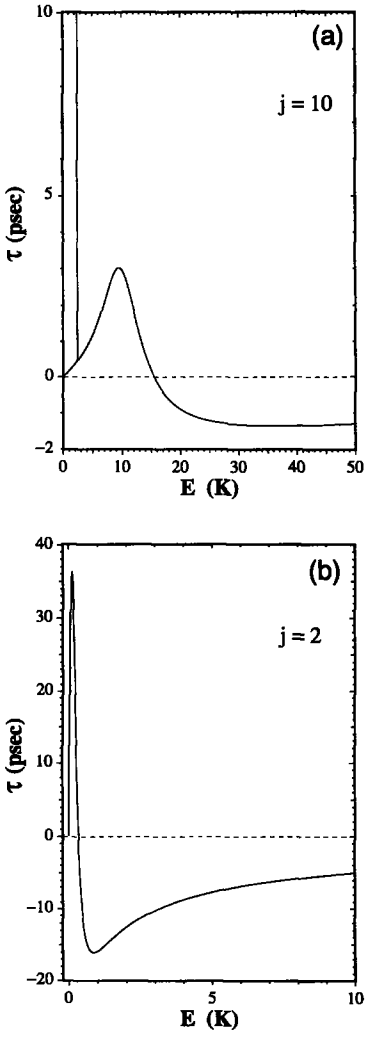

Fig. 2. Collision lifetimes (delay times) (in picoseconds) versus energy (in Kelvin) of the continuum states of Ne_2. (a) $j = 10$. At this angular momentum there is both a narrow quasibound resonant state and a broad above barrier resonance. (b) $j = 2$. Here there is only a low-energy barrier exclusion resonance, and τ is elsewhere negative (nonresonant).

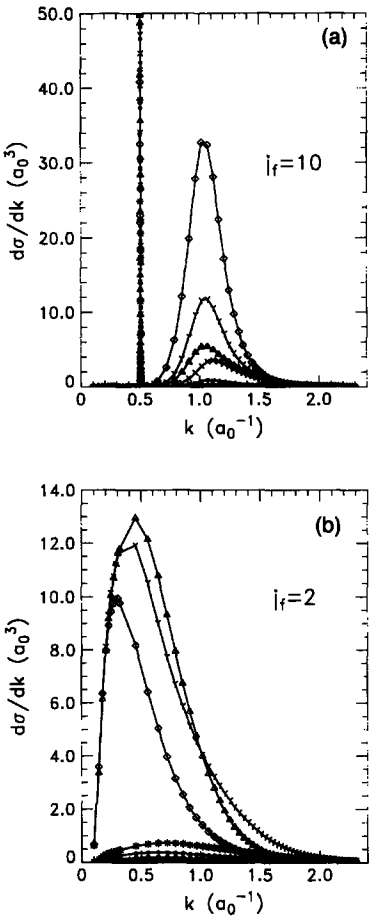

Fig. 3. $d\sigma/dk$ versus k (atomic units). The area under each curve is the bound-free integral cross section, so that this plot shows the contribution of a given energy of relative motion of the *Ne* atoms. The symbols label the initial states, $i = (v,j)$: solid circles, (0,0); asterisks, (0,2); solid squares, (0,4); solid triangles, (0,6); X, (0,8); open triangles, (1,0); Y, (1,2); and diamonds, (1,4). (a) $j_f = 10$. Contributions of the quasibound and broad above barrier resonances. (b) $j_f = 2$. Contributions of the nonresonant three-body continuum.

the $j_f = 8$ contribution is mostly a BAB resonance; and the $j_f \geq 14$ contributions are mostly due to BAB resonances that become so broad as to merge into the nonresonant continuum.

The integration of $d\sigma/dk$ over k to get integral cross sections was performed using trapezoidal rule quadrature. In this process, it was observed that the narrow quasibound contributions approach δ function behavior. As the resonance narrows, the maximum in $d\sigma/dk$ gets large, but its integral over k

Table 2
Cross sections (a_0^2) at $E/k_B = 30$ K from all bound states i = (v,j) into the quasibound (0,10) resonant state treated as a scattering (s) or bound (b) state

f ← i	(0,0)	(0,2)	(0,4)	(0,6)	(0,8)	(1,0)	(1,2)	(1,4)
(0,10)(s) ← i	0.42	0.98	4.14	16.98	48.29	0.19	0.43	1.02
(0,10)(b) ← i	0.42	0.97	4.10	16.83	47.85	0.19	0.43	1.02

approaches a constant. To see if it approaches the contribution of a bound state, calculations were done in which the wavefunctions of the very narrow (0,10) QB resonance were replaced by a square-integrable wavefunction which is proportional to the wavefunction of Fig. 1 out to its first node, zero thereafter, and normalized to unity. The results are compared in Table 2, and one sees that, to the accuracy with which the continuum quadrature was done, they are identical. Hence, the contributions of this narrow resonance can be obtained either by integrating over its continuum wavefunctions or by simply approximating it as a bound state. This approach was also used to approximately separate the QB contributions from the BAB and 3B contributions in the cases [(1,6) and (0,12)] where they are not so easily separated as for (0,10). Square-integrable wavefunctions were normalized out to the appropriate number of nodes, and the results were subtracted from the total for that j_f.

The resulting integral cross sections are in Table 3. The columns are labeled by the initial states, the rows by the final states. The last three columns are cross sections out of the square-integrable approximations to the QB states. The upper left 8 by 8 matrix shows that the bound-bound cross sections

Table 3
Cross sections (a_0^2) at $E/k_B = 30$ K from states i = (v,j) into states f = (v',j')

f ← i	(0,0)	(0,2)	(0,4)	(0,6)	(0,8)	(1,0)	(1,2)	(1,4)	(1,6)	(0,10)	(0,12)
(0,0)	360.08	19.07	4.59	.78	.12	.89	.15	.01	.00	.02	.00
(0,2)	95.34	398.97	34.93	8.52	1.49	.76	1.16	.27	.02	.23	.04
(0,4)	41.33	62.87	392.92	37.03	9.69	.56	.66	1.08	.19	1.76	.24
(0,6)	10.12	22.14	53.48	391.07	38.30	.76	.66	.60	.66	10.42	1.78
(0,8)	1.97	5.08	18.30	50.09	389.93	.44	.68	.78	.48	38.74	10.06
(1,0)	.89	.15	.06	.06	.03	360.71	15.16	5.51	1.34	.01	.00
(1,2)	.75	1.16	.37	.25	.20	75.82	398.08	32.02	8.84	.10	.05
(1,4)	.12	.48	1.08	.42	.41	49.62	57.63	396.47	27.00	.44	.36
(1,6)	.06	.06	.28	.66	.36	17.38	22.98	39.01	402.05	.61	1.12
(0,10)	.42	.97	4.10	16.83	47.85	.19	.43	1.02	.98	388.64	36.11
(0,12)	.09	.18	.68	3.42	14.79	.09	.26	1.01	2.15	42.99	386.95
(k,0)	.62	.08	.04	.02	.00	4.55	1.67	.77	1.13	.00	.01
(k,2)	.44	.88	.21	.12	.05	9.28	9.04	5.47	6.98	.02	.06
(k,4)	.18	.41	1.06	.30	.22	6.49	9.00	11.97	14.03	.10	.13
(k,6)	.18	.15	.58	1.58	.58	7.56	11.26	15.59	.00	.59	.55
(k,8)	.10	.11	.18	1.06	2.56	8.62	14.37	28.72	54.31	1.62	3.73
(k,10)	.04	.07	.12	.40	1.78	2.63	4.83	12.49	29.11	3.46	5.22
(k,12)	.03	.05	.13	.41	1.59	.78	1.40	4.05	13.40	4.37	.00
(k,14)	.04	.06	.19	.77	3.94	.29	.54	1.82	7.48	17.24	48.38
(k,16)	.01	.02	.05	.16	.75	.10	.19	.67	3.53	4.21	19.06
(k,18)	.00	.00	.01	.02	.08	.03	.06	.26	1.70	.57	4.83
(k,20)	.00	.00	.00	.00	.00	.01	.02	.09	.83	.03	.74

Table 4
Total cross sections (a_0^2) for possible processes of a given type at $E/k_B = 30$ K from states i = (v,j)

f ← i	(0,0)	(0,2)	(0,4)	(0,6)	(0,8)	(1,0)	(1,2)	(1,4)
i ← i	360.08	398.97	392.92	391.07	389.93	360.71	398.08	396.47
b ← i	150.52	110.96	112.81	97.14	50.24	128.85	76.11	40.27
QB ← i	.57	1.21	5.06	20.90	63.01	17.66	23.66	41.03
BAB ← i	.40	.47	1.25	4.38	11.29	20.02	32.67	63.69
3B ← i	1.24	1.37	1.31	.44	.27	20.31	19.71	18.21
tot(sum) ← i	512.82	512.98	513.34	513.92	514.74	547.54	550.24	559.67
tot(com) ← i	512.90	513.07	513.48	514.24	515.58	549.41	552.52	563.39

have the physically expected behavior: Vibrationally inelastic cross sections are small, and rotationally inelastic cross sections are largest for small Δj transitions. Lines 8 through 11 are cross sections for transitions between the bound and the quasibound states. They are about the same size as the bound-bound cross sections. Lines 12 through 22 are cross sections for transitions to all the continuum states except the quasibound states. Again, they are similar to the bound-bound cross sections. In particular, the cross sections to the nonresonant true 3B continuum states with $j_f = 0$, 2, and 4 are very nearly as large as those to the BAB and QB resonances.

This last observation is clarified by Table 4. There, the sums of cross sections for transitions of a particular type from each of the bound states are presented; namely, the rows are elastic, total bound-bound inelastic, total bound-quasibound, total bound-broad above barrier, and total bound-direct three-body continuum. For the bound states that have significant cross sections to unbound states, it is clear that all three types of unbound states are important; none can be omitted.

The last two lines of Table 4 are a numerical check. The upper is the sum of its column of Table 4 (or Table 3). The lower is the total integral cross section evaluated using the completeness relation. Their very good agreement verifies that our numerical calculations are accurate and that the set of states included is complete.

4. Conclusions

This Letter presents cross sections relevant to recombination and collision-induced dissociation (CID) obtained using a VRIOS approximation which should be qualitatively to semiquantitatively accurate, which treats all the bound and continuum states on an equal footing and which should not favor any type of state.

The results show clearly that *three* types of continuum states all contribute significantly to the reaction: quasibound states, broad above barrier resonances, and nonresonant three-body continuum states. All three must be included in the kinetics.

The present results constitute the first clear quantum mechanical evidence that nonresonant, direct three-body collisions do contribute significantly to recombination and CID along with the sequential two-body collisions. Work is in progress [6] to generate rate coefficients and do master equation kinetics to provide even more detail about how much of the reaction goes via each mechanism.

Acknowledgements

This work was performed under the auspices of the US Department of Energy under the Laboratory Directed Research and Development Program.

References

[1] See, for example, J. Troe, Physical Chem.: An Advanced Treatise B 6 (1975) 835.
[2] See, for example, C.J. Cobos, H. Hippler, J. Troe, J. Phys. Chem. 89 (1985) 342; R. Forster, M. Frost, D. Fulle, H.F. Hamann, H. Hippler, A. Schlepegrell, J. Troe, J. Chem. Phys. 103 (1995) 2949.
[3] R.J. Duchovic, J.D. Pettigrew, B. Walling, T. Shipchandler, J. Chem. Phys. 105 (1996) 10367.
[4] R.E. Roberts, R.B. Bernstein, C.F. Curtiss, J. Chem. Phys. 50

(1969) 5163; P.A. Whitlock, J.T. Muckerman, R.E. Roberts, J. Chem. Phys. 60 (1974) 3658, and references therein.
[5] F.T. Smith, in: Kinetic Processes in Gases and Plasmas, Ed. A.R. Hochstim (Academic, New York, 1969) pp. 321–381.
[6] R.T Pack, R.B. Walker, B. Kendrick (unpublished work).
[7] R.E. Roberts, J. Chem. Phys. 54 (1971) 1422; M. Menzinger, Chem. Phys. Lett. 10 (1971) 507.
[8] L.P. Walkauskas, F. Kaufman, J. Chem. Phys. 64 (1976) 3885; D.N. Mitchell, D.J. LeRoy, J. Chem. Phys. 67 (1977) 1042.
[9] See, for example, D.L. Martin, L.M. Raff, D.L. Thompson, J. Chem. Phys. 92 (1990) 5311, and references therein.
[10] See K. Haug, D.G. Truhlar, N.C. Blais, J. Chem. Phys. 86 (1987) 2697; 96 (1992) 5556; S. Kumar, N. Sathyamurthy, Chem. Phys. 137 (1989) 25.
[11] D.W. Schwenke, J. Chem. Phys. 89 (1988) 2076.
[12] D.W. Schwenke, J. Chem. Phys. 92 (1990) 7267.
[13] W.H. Miller, J. Phys. Chem. 99 (1995) 12387; V.A. Mandelshtam, H.S. Taylor, W.H. Miller, J. Chem. Phys. 105 (1995) 496.
[14] K. Nobusada, K. Sakimoto, Chem. Phys 197 (1995) 147; J. Chem. Phys. 106 (1997) 9078.
[15] B. Pan, J.M. Bowman, J. Chem. Phys. 103 (1995) 9661.
[16] G.A. Pfeffer, J. Phys. Chem. 89 (1985) 1131.
[17] G.A. Parker, R.T Pack, J. Chem. Phys. 68 (1978) 1585.
[18] R.A. Aziz, M.J. Slaman, Chem. Phys. 130 (1989) 187.
[19] W.J. Meath, R.A. Aziz, Mol. Phys. 52 (1984) 225.
[20] K.T. Tang, J.P. Toennies, Chem. Phys. 156 (1991) 413.
[21] B.R. Johnson, J. Chem. Phys. 67 (1977) 4086.
[22] R.B. Walker, E.F. Hayes, J. Chem. Phys. 91 (1990) 4106.
[23] B. Kendrick, R.T Pack, J. Chem. Phys. 104 (1996) 7502.